ChemComm

Cite this: *Chem. Commun.*, 2012, **48**, 6493–6495

www.rsc.org/chemcomm

COMMUNICATION

A robust doubly interpenetrated metal–organic framework constructed from a novel aromatic tricarboxylate for highly selective separation of small hydrocarbons†

Yabing He,*[a] Zhangjing Zhang,[ab] Shengchang Xiang,[ab] Frank R. Fronczek,[c] Rajamani Krishna*[d] and Banglin Chen*[a]

Received 10th March 2012, Accepted 8th May 2012
DOI: 10.1039/c2cc31792c

A microporous metal–organic framework, for the first time, has been developed for highly selective separation of industrially important C_1, C_2 and C_3 hydrocarbons at room temperature.

The research of new materials for highly selective gas separation is of significant importance for development of more efficient and economical ways to purify industrially important gases. As an emerging class of porous materials, metal–organic frameworks (MOFs) have recently shown great promise in this aspect.[1] This is mainly because the micropores within MOFs can be systematically tuned by selecting the diverse metal-containing secondary building units (SBUs) and the rich organic linkers[2] and/or by making use of the framework interpenetration.[3] Furthermore, the separation selectivity can be improved by immobilization of different recognition sites on pore surfaces such as open metal sites, organic functional groups to direct their different recognition for gas molecules.[4–6]

During the course of MOF development, the use of C_3-symmetric tritopic carboxylate linkers turns out to be very useful in constructing porous MOF materials.[7–10] For instance, the benchmark MOF **HKUST-1** is built from the smallest aromatic tricarboxylates H_3BTC (benzene-1,3,5-tricarboxylic acid) and the $Cu_2(COO)_4$ clusters, showing the interesting diverse properties for gas storage/separation, catalysis and proton conductivity.[9] Incorporation of the elongated versions H_3BTB (4,4′,4″-benzene-1,3,5-triyl-tribenzoic acid), H_3BBC (4,4′,4″-(benzene-1,3,5-triyl-tris(benzene-4,1-diyl))tribenzoic acid) with the $Zn_4O(COO)_6$ clusters produces **MOF-177** and **MOF-200**, respectively, which exhibit excellent gas storage capacity.[10] In light of these observations, we have designed and prepared a much aromatic-richer analogue H_3BTN (6,6′,6″-benzene-1,3,5-triyl-2,2′,2″-trinaphthoic acid, Scheme 1) and constructed a microporous MOF (which we term **UTSA-35**, UTSA = University of Texas at San Antonio) with double framework interpenetration. The desolvated framework **UTSA-35a** exhibits highly selective separation of industrially important small hydrocarbons at room temperature.

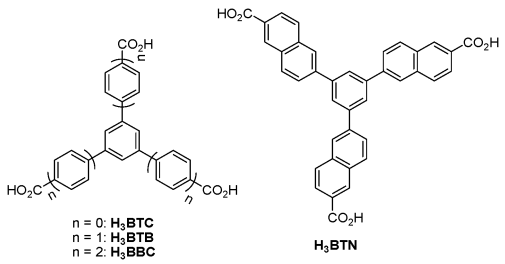

Scheme 1 Molecular structures of the organic linkers H_3BTC, H_3BTB, H_3BBC, and H_3BTN.

The organic linker H_3BTN was readily synthesized by Pd-catalyzed Suzuki cross-coupling between methyl 6-(pinacolboryl)-2-naphthoate and 1,3,5-tribromobenzene followed by base-catalyzed hydrolysis (see ESI†). **UTSA-35** was obtained as yellowish block-shaped crystals *via* a solvothermal reaction of H_3BTN and $Cd(NO_3)_2{\cdot}4H_2O$ in *N*,*N*′-dimethylformamide (DMF) at 100 °C for 24 h. The structure was determined by single-crystal X-ray diffraction analysis, and the phase purity of the bulk material was confirmed by powder X-ray diffraction (PXRD, Fig. S1, ESI†). **UTSA-35** can be formulated as $Cd_3(BTN)_2(H_2O)_3(DMF)_6$ on the basis of single-crystal X-ray diffraction structure determination, thermogravimetric analysis (TGA), and microanalysis. TGA shows that **UTSA-35** can be thermally stable up to 360 °C under a nitrogen atmosphere (Fig. S2, ESI†).

X-ray crystallography reveals that **UTSA-35** possesses a two-fold interpenetrated three–dimensional (3D) network that crystallizes in the monoclinic $P2_1/c$ space group.‡ The asymmetric unit contains three Cd centers, two deprotonated ligands, three coordinated water molecules, one terminal DMF and five free DMF molecules. Three carboxylate groups of the

[a] *Department of Chemistry, University of Texas at San Antonio, One UTSA Circle, San Antonio, Texas 78249-0698, USA. E-mail: Yabing.He@utsa.edu, Banglin.Chen@utsa.edu; Fax: +1-210-458-7428*
[b] *College of Chemistry and Materials, Fujian Normal University, 3 Shangsan Road, Cangshang Region, Fuzhou, China 350007*
[c] *Department of Chemistry, Louisiana State University, Baton Rouge, LA 70803-1804, USA*
[d] *Van 't Hoff Institute of Molecular Science, University of Amsterdam, Science Park 904, 1098 XH Amsterdam, The Netherlands. E-mail: r.krishna@uva.nl*

† Electronic supplementary information (ESI) available: Synthesis and characterization of H_3BTN and **UTSA-35**, PXRD, TGA, sorption isotherms, FTIR. CCDC 868753. For ESI and crystallographic data in CIF or other electronic format see DOI: 10.1039/c2cc31792c

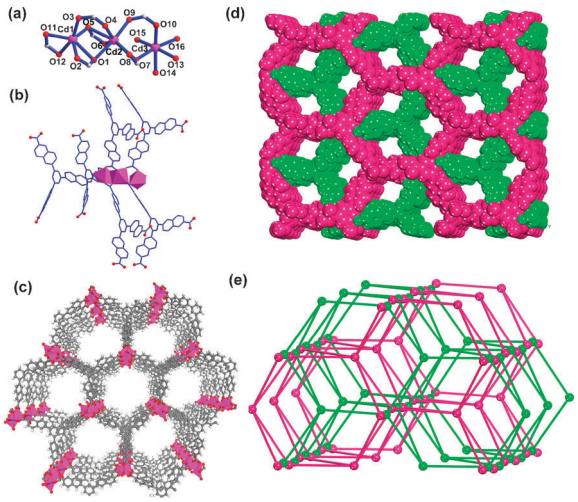

Fig. 1 Single-crystal X-ray structure of **UTSA-35** indicating the trinuclear cadmium–carboxylate secondary building unit (a) linked by six organic ligands (b), the single net (c) and two-fold interpenetrated net (d) showing the channel along *a* axis, and (3,6)-connected topology with Schläfli symbol of $(4^16^2)_2(4^26^{10}8^3)$ (e). Hydrogen atoms are omitted for clarity.

organic linker adopt different coordination modes: chelating (η^2), bridging (μ_2–η^1:η^1) and chelating–bridging (μ_2–η^2:η^1), respectively (Fig. S3, ESI†). The secondary building unit (SBU) is a tricadmium–carboxylate cluster where Cd1, Cd2 and Cd3 atoms are six-, seven- and six-coordinated, respectively (Fig. 1a and b). The overall topology is a (3,6)-connected binodal $(4^16^2)_2(4^26^{10}8^3)$ net if the organic linker and the metal-containing cluster are taken as 3-connected and 6-connected nodes, respectively (Fig. 1e). There exist hexagonal channels in the single net along the *a* direction with the approximate dimensions of 11 Å (Fig. 1c). Due to the large void, two such nets interpenetrate each other *via* intermolecular π···π interactions between the central benzene rings (Fig. 1d). As a result, the stability of the whole structure is enhanced and the porosity of the framework is further tuned. The hexagonal channels are dissected into smaller tetragonal channels with the dimensions of 7.7 × 5.8 Å, taking into account the van der Waals radii. The void space accounts approximately 45.8% of the whole crystal volume as estimated by PLATON.

To characterize the permanent porosity, nitrogen and hydrogen adsorption experiments were performed at 77 K. The fresh sample was guest-exchanged with dry acetone and then outgassed under high vacuum at 333 K to generate desolvated **UTSA-35a**. The PXRD pattern of **UTSA-35a** is similar to that of the pristine sample (Fig. S1, ESI†), indicating that the framework is maintained after the removal of the solvent molecules. The N_2 sorption isotherm at 77 K displays a type I reversible sorption behavior typical for microporous materials with Brunauer–Emmett–Teller (BET) and Langmuir surface areas of 742.7 and 758.4 $m^2\ g^{-1}$, respectively, and a pore volume of 0.313 $cm^3\ g^{-1}$ (Fig. S4 and S5, ESI†). The hydrogen isotherm at 77 K shows that **UTSA-35a** takes up 1.1 wt% H_2 at 1 atm (Fig. S6, ESI†).

Establishment of permanent microporosity encourages us to examine its utility as an adsorbent for industrially important small hydrocarbon separation. The pure component sorption isotherms for various hydrocarbons were measured (Fig. S7, ESI†).

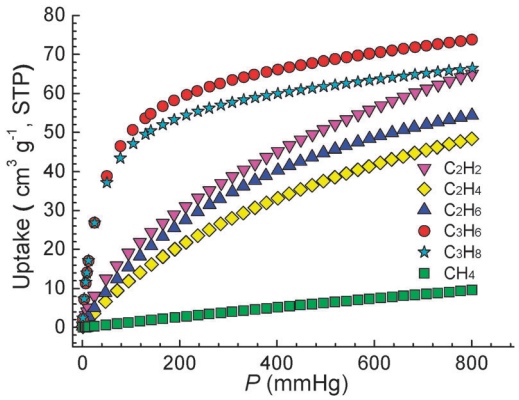

Fig. 2 Single-component sorption isotherms for various hydrocarbons in **UTSA-35a** at 296 K.

As shown in Fig. 2, **UTSA-35a** takes up different amounts of C_3H_8 (130.8 mg g^{-1}), C_3H_6 (138.5 mg g^{-1}), C_2H_6 (73.0 mg g^{-1}), C_2H_4 (60.6 mg g^{-1}), C_2H_2 (75.6 mg g^{-1}) and CH_4 (6.9 mg g^{-1}) at 296 K and 1 atm. The most striking feature is that **UTSA-35a** exhibits adsorption capacity in the following trend: $C_3 > C_2 > C_1$, highlighting **UTSA-35a** as a promising material not only for separation of higher hydrocarbons from CH_4 but also for selective fractionation of these small hydrocarbons according to the number of carbon atoms.

The adsorption selectivities of different hydrocarbons with respect to CH_4 in an equimolar 6-component mixture were calculated using ideal solution adsorbed theory (IAST) of Myers and Prausnitz.[11] The accuracy of IAST for prediction of gas mixture adsorption in many zeolites and MOF materials has been established in a number of publications in the literature.[12] As shown in Fig. 3, the selectivities of C_3 and C_2 components with respect to CH_4 are in excess of 80 and 8, respectively, for a range of pressures of up to 100 kPa. Fractionation of these hydrocarbons is expected to be practically feasible.

To further demonstrate the feasibility, the breakthrough experiments were simulated using the established methodology described in the work of Krishna and Long.[13] Assuming the isotherm condition, with the adsorber maintained at 296 K,

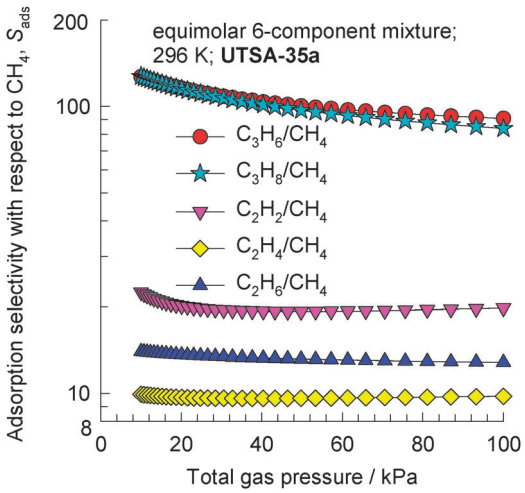

Fig. 3 IAST calculations of adsorption selectivities of different hydrocarbons with respect to CH_4 in an equimolar 6-component mixture at 296 K in **UTSA-35a**.

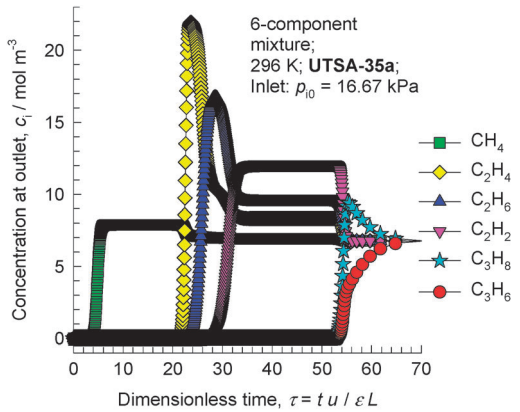

Fig. 4 The simulated transient breakthrough of an equimolar 6–component mixture containing C_3H_8, C_3H_6, C_2H_6, C_2H_4, C_2H_2, and CH_4 in an adsorber packed with **UTSA-35a**, operating under isothermal conditions at 296 K. The inlet gas is maintained at partial pressures P_{i0} = 16.67 kPa.

the transient breakthrough of an equimolar 6-component mixture containing CH_4, C_2H_2, C_2H_4, C_2H_6, C_3H_6 and C_3H_8 was determined. The molar concentrations of the gas phase exiting the adsorber are shown in Fig. 4 for a gas mixture with partial pressures of 16.67 kPa each for each of the six components in the inlet. From the breakthrough curves, we note that CH_4, the component with the poorest adsorption strength, breaks through earliest, followed by the C_2 components with the moderate adsorption strength and finally by C_3 components with the strongest adsorption strength. Therefore it is possible to fractionate the mixture into three separate streams: CH_4, C_2 hydrocarbons and C_3 hydrocarbons during the adsorption cycle.

In summary, we design a novel expanded and decorated ligand and synthesize a robust doubly interpenetrated metal–organic framework for fractionation of C_1, C_2 and C_3 hydrocarbons. This is the first example of porous metal–organic frameworks for such industrially important hydrocarbon separation.[14,15] The interactions between the MOF material and hydrocarbons are mainly van der Waals interactions which favor the stronger adsorption of higher hydrocarbons. The size-selective effect plays an important role in the separation of C_2H_2/C_2H_4 and C_2H_2/C_2H_6. It is expected that this work will stimulate more investigation of newly emerging microporous metal–organic frameworks for separation of industrially important small hydrocarbons and eventually some practically useful MOF materials will be targeted in the future.

This work was supported by an AX-1730 from Welch Foundation (BC).

Notes and references

‡ Crystal data for **UTSA-35**: $C_{96}H_{90}Cd_3N_6O_{21}$, M = 2001.00, monoclinic, space group $P2_1/c$, a = 14.306(2) Å, b = 19.509(3) Å, c = 36.482(5) Å, β = 99.6290(9)°, V = 10039(2) Å^3, Z = 4, D_c = 1.324 g cm^{-3}, μ(Mo-K$_\alpha$) = 0.683 mm^{-1}, F(000) = 3440, final R_1 = 0.0594 for $I > 2\sigma(I)$, wR_2 = 0.1744 for all data, GoF = 1.022, CCDC 868753.

1 (*a*) J.-R. Li, J. Sculley and H.-C. Zhou, *Chem. Rev.*, 2012, **112**, 869; (*b*) K. Sumida, D. L. Rogow, J. A. Mason, T. M. McDonald, E. D. Bloch, Z. R. Herm, T.-H. Bae and J. R. Long, *Chem. Rev.*, 2012, **112**, 724; (*c*) Y.-S. Bae and R. Q. Snurr, *Angew. Chem., Int. Ed.*, 2011, **50**, 11586; (*d*) H. Wu, Q. Gong, D. H. Olson and J. Li, *Chem. Rev.*, 2012, **112**, 836; (*e*) S. Kitagawa, R. Kitaura and S.-I. Noro, *Angew. Chem., Int. Ed.*, 2004, **43**, 2334; (*f*) H.-L. Jiang and Q. Xu, *Chem. Commun.*, 2011, **47**, 3351; (*g*) B. Chen, S. Xiang and G. Qian, *Acc. Chem. Res.*, 2010, **43**, 1115; (*h*) Z. Zhang, S. Xiang and B. Chen, *CrystEngComm*, 2011, **13**, 5983.

2 M. Eddaoudi, J. Kim, N. Rosi, D. Vodak, J. Wachter, M. O'Keeffe and O. M. Yaghi, *Science*, 2002, **295**, 469.

3 (*a*) B. Chen, C. Liang, J. Yang, D. S. Contreras, Y. L. Clancy, E. B. Lobkovsky, O. M. Yaghi and S. Dai, *Angew. Chem., Int. Ed.*, 2006, **45**, 1390; (*b*) B. Chen, S. Ma, F. Zapata, F. R. Fronczek, E. B. Lobkovsky and H.-C. Zhou, *Inorg. Chem.*, 2007, **46**, 1233.

4 (*a*) Y.-S. Bae, O. K. Farha, A. M. Spokoyny, C. A. Mirkin, J. T. Hupp and R. Q. Snurr, *Chem. Commun.*, 2008, 4135; (*b*) R. Vaidhyanathan, S. S. Iremonger, G. K. H. Shimizu, P. G. Boyd, S. Alavi and T. K. Woo, *Science*, 2010, **330**, 650; (*c*) J. An, S. J. Geib and N. L. Rosi, *J. Am. Chem. Soc.*, 2010, **132**, 38; (*d*) T. Panda, P. Pachfule, Y. Chen, J. Jiang and R. Banerjee, *Chem. Commun.*, 2011, **47**, 2011; (*e*) J.-P. Zhang and X.-M. Chen, *J. Am. Chem. Soc.*, 2009, **131**, 5516; (*f*) Q. Lin, T. Wu, S.-T. Zheng, X. Bu and P. Feng, *J. Am. Chem. Soc.*, 2012, **134**, 784; (*g*) Y.-X. Tan, Y.-P. He and J. Zhang, *Chem. Commun.*, 2011, **47**, 10647; (*h*) Z. Chen, S. Xiang, H. D. Arman, J. U. Mondal, P. Li, D. Zhao and B. Chen, *Inorg. Chem.*, 2011, **50**, 3442.

5 D. Britt, H. Furukawa, B. Wang, T. G. Glover and O. M. Yaghi, *Proc. Natl. Acad. Sci. U. S. A.*, 2009, **106**, 20637.

6 Y.-S. Bae, C. Y. Lee, K. C. Kim, O. K. Farha, P. Nickias, J. T. Hupp, S. T. Nguyen and R. Q. Snurr, *Angew. Chem., Int. Ed.*, 2012, **51**, 1857.

7 (*a*) B. Chen, M. Eddaoudi, S. T. Hyde, M. O'Keeffe and O. M. Yaghi, *Science*, 2001, **291**, 1021; (*b*) K. Koh, A. G. Wong-Foy and A. J. Matzger, *Angew. Chem., Int. Ed.*, 2008, **47**, 677; (*c*) K. Gedrich, I. Senkovska, N. Klein, U. Stoeck, A. Henschel, M. R. Lohe, I. A. Baburin, U. Mueller and S. Kaskel, *Angew. Chem., Int. Ed.*, 2010, **49**, 8489; (*d*) S.-T. Zheng, J. J. Bu, T. Wu, C. Chou, P. Feng and X. Bu, *Angew. Chem., Int. Ed.*, 2011, **50**, 8858.

8 (*a*) S. Ma and H.-C. Zhou, *J. Am. Chem. Soc.*, 2006, **128**, 11734–11735; (*b*) Y. K. Park, S. B. Choi, H. Kim, K. Kim, B.-H. Won, K. Choi, J.-S. Choi, W.-S. Ahn, N. Won, S. Kim, D. H. Jung, S.-H. Choi, G.-H. Kim, S.-S. Cha, Y. H. Jhon, J. K. Yang and J. Kim, *Angew. Chem., Int. Ed.*, 2007, **46**, 8230.

9 (*a*) S. S.-Y. Chui, S. M.-F. Lo, J. P. H. Charmant, A. G. Orpen and I. D. Williams, *Science*, 1999, **283**, 1148; (*b*) B. Xiao, P. S. Wheatley, X. Zhao, A. J. Fletcher, S. Fox, A. G. Rossi, I. L. Megson, S. Bordiga, L. Regli, K. M. Thomas and R. E. Morris, *J. Am. Chem. Soc.*, 2007, **129**, 1203; (*c*) S. Xiang, W. Zhou, J. M. Gallegos, Y. Liu and B. Chen, *J. Am. Chem. Soc.*, 2009, **131**, 12415; (*d*) C.-Y. Sun, S.-X. Liu, D.-D. Liang, K.-Z. Shao, Y.-H. Ren and Z.-M. Su, *J. Am. Chem. Soc.*, 2009, **131**, 1883; (*e*) N. C. Jeong, B. Samanta, C. Y. Lee, O. K. Farha and J. T. Hupp, *J. Am. Chem. Soc.*, 2012, **134**, 51.

10 (*a*) H. K. Chae, D. Y. Siberio-Pérez, J. Kim, Y. Go, M. Eddaoudi, A. J. Matzger, M. O'Keeffe and O. M. Yaghi, *Nature*, 2004, **427**, 523; (*b*) H. Furukawa, N. Ko, Y. B. Go, N. Aratani, S. B. Choi, E. Choi, A. Ö. Yazaydin, R. Q. Snurr, M. O'Keeffe, J. Kim and O. M. Yaghi, *Science*, 2010, **329**, 424.

11 A. L. Myers and J. M. Prausnitz, *AIChE J.*, 1965, **11**, 121.

12 (*a*) R. Krishna, S. Calero and B. Smit, *Chem. Eng. J.*, 2002, **88**, 81; (*b*) R. Krishna and J. M. van. Baten, *Chem. Eng. J.*, 2007, **133**, 121; (*c*) R. Krishna and J. M. van. Baten, *Phys. Chem. Chem. Phys.*, 2011, **13**, 10593; (*d*) R. Krishna and J. M. van. Baten, *J. Membr. Sci.*, 2011, **377**, 249.

13 R. Krishna and J. R. Long, *J. Phys. Chem. C*, 2011, **115**, 12941.

14 (*a*) M. C. Das, H. Xu, S. Xiang, Z. Zhang, H. D. Arman, G. Qian and B. Chen, *Chem.–Eur. J.*, 2011, **17**, 7817; (*b*) S. Xiang, Z. Zhang, C.-G. Zhao, K. Hong, X. Zhao, D.-L. Ding, M.-H. Xie, C.-D. Wu, R. Gill, K. M. Thomas and B. Chen, *Nat. Commun.*, 2011, **2**, 204; (*c*) Y. He, S. Xiang and B. Chen, *J. Am. Chem. Soc.*, 2011, **133**, 14570; (*d*) Y. He, Z. Zhang, S. Xiang, F. R. Fronczek, R. Krishna and B. Chen, *Chem.–Eur. J.*, 2012, **18**, 613; (*e*) Y. He, Z. Zhang, S. Xiang, H. Wu, F. R. Fronczek, W. Zhou, R. Krishna, M. O'Keeffe and B. Chen, *Chem.–Eur. J.*, 2012, **18**, 1901.

15 E. D. Bloch, W. L. Queen, R. Krishna, J. M. Zadrozny, C. M. Brown and J. R. Long, *Science*, 2012, **335**, 1606.

Supporting Information

A robust doubly interpenetrated metal–organic framework constructed from a novel aromatic tricarboxylate for highly selective separation of small hydrocarbons

Yabing He,[a] Zhangjing Zhang,[a] Shengchang Xiang,[a] Frank R. Fronczek,[b] Rajamani Krishna, *,[c] and Banglin Chen*[a]

[a] Department of Chemistry, University of Texas at San Antonio, One UTSA Circle, San Antonio, Texas 78249-0698, United States; Fax: (1)-210-458-7428; E-mail: Banglin.Chen@utsa.edu; Homepage: www.utsa.edu/chem/chen.htlm

[b] Department of Chemistry, Louisiana State University, Baton Rouge, LA 70803-1804, United States.

[c] Van 't Hoff Institute for Molecular Sciences, University of Amsterdam, Science Park 904, 1098 XH Amsterdam, The Netherlands

General remark

All reagents and solvents were used as received from commercial suppliers without further purification. ^{1}H NMR and ^{13}C NMR spectra were recorded on a Varian Mercury 300 MHz spectrometer. Tetramethylsilane (TMS) and deuterated solvents ($CDCl_3$, δ = 77.0 ppm; DMSO-d_6, δ = 39.5 ppm) were used as internal standards in ^{1}H NMR and ^{13}C NMR experiments, respectively. The coupling constants were reported in Hertz. FTIR spectra were performed on a Bruker Vector 22 spectrometer at room temperature. The elemental analyses were performed with Perkin–Elmer 240 CHN analyzers from Galbraith Laboratories, Knoxville. Thermogravimetric analyses (TGA) were measured using a Shimadzu TGA-50 analyzer under a nitrogen atmosphere with a heating rate of 3 ^{o}C min^{-1}. Powder X–ray diffraction (PXRD) patterns were recorded by a Rigaku Ultima IV diffractometer operated at 40 kV and 44 mA with a scan rate of 1.0 deg min^{-1}. The crystallographic measurement was made on a Bruker SMART Apex II CCD–based X–ray diffractometer system equipped with a Mo–target X-ray tube (λ = 0.71073 Å) operated at 2000 watts power (50 kV, 40 mA). The structure was solved by direct method and refined to convergence by least squares method on F^2 using the SHELXTL software suit. A Micromeritics ASAP 2020 surface area analyzer was used to measure gas adsorption isotherms. To have a guest–free framework, the fresh sample was guest–exchanged with

dry acetone at least 10 times, filtered and vacuumed at 60 ^{o}C until the outgas rate was 5 μmHg min^{-1} prior to measurements. A sample of 102.6 mg was used for the sorption measurements and was maintained at 77 K with liquid nitrogen, at 273 K with an ice–water bath. As the center–controlled air conditioner was set up at 23 ^{o}C, a water bath was used for adsorption isotherms at 296 K.

Fits of pure-component isotherms

The measured experimental data on pure–component isotherms for CH_4, C_2H_2, C_2H_4, C_2H_6, C_3H_6, C_3H_8 at 273 K, and 296 K in the **UTSA-35a** were first converted to absolute loadings using the Peng–Robinson equation of state for estimation of the fluid densities. The experimentally measured pore volume of 0.3133 cm^3 g^{-1} was used for this purpose. Depending on the guest-host combination, the isotherm model of choice is either a 1-site Langmuir (SSL) model:

$$q = \frac{q_{sat} bp}{1+bp};\ b = b_0 \exp\left(\frac{E}{RT}\right)$$

or a 2-site Langmuir (DSL) model

$$q \equiv q_A + q_B = \frac{q_{sat,A} b_A p}{1+b_A p} + \frac{q_{sat,B} b_B p}{1+b_B p};\ b_A = b_{A0} \exp\left(\frac{E_A}{RT}\right);\ b_B = b_{B0} \exp\left(\frac{E_B}{RT}\right)$$

The selected isotherm models along with the fit parameters are specified in *Table S2*. *Figure S8* compares the experimental loadings with the isotherm fits for each hydrocarbon species. There is excellent agreement for each species over the entire range of pressures at both temperatures.

Isosteric heats of adsorption

The isosteric heat of adsorption, Q_{st}, defined as

$$Q_{st} = RT^2 \left(\frac{\partial \ln p}{\partial T}\right)_q$$

was determined using the pure–component isotherm fits. The procedure for calculation of Q_{st} is the same as that described in the Supporting Information accompanying the paper by Mason et al.[1] Q_{st} is

a function of the loading. The loading dependences of Q_{st} for various hydrocarbons are compared in *Figure S9*.

IAST calculations of adsorption selectivities

In order to determine the adsorption selectivities of different hydrocarbons C_2H_2, C_2H_4, C_2H_6 , C_3H_6, C_3H_8 with respect to CH_4, 6–component mixture adsorption equilibrium was determined using the Ideal Adsorbed Solution Theory (IAST) of Myers and Prausnitz.[2] The bulk gas phase was assumed to be equimolar, with equal partial pressures of each of the six components. For each of the hydrocarbons, using the pure component isotherm fits, the adsorption selectivities were determined from

$$S_{ads} = \frac{q_{Hydrocarbon} / q_{CH4}}{p_{Hydrocarbon} / p_{CH4}}$$

The accuracy of the IAST calculations for estimation of the component loadings for several binary mixtures in a wide variety of zeolites, and MOF materials has been established by comparison with Configurational-Bias Monte Carlo (CBMC) simulations of mixture adsorption.[3-5]

Breakthrough calculations

In order to demonstrate the feasibility of the use of **UTSA-35a** for separation of CH_4 from other hydrocarbons in a PSA unit, we performed transient breakthrough calculations following the methodologies developed and described in earlier works.[6-8] *Figure S10* shows a schematic of a packed bed adsorber. Assuming plug flow of the gas mixture through the fixed bed maintained under isothermal conditions and negligible pressure drop, the partial pressures in the gas phase at any position and instant of time are obtained by solving the following set of partial differential equations for each of the species *i* in the gas mixture.

$$\frac{1}{RT}\varepsilon\frac{\partial p_i(t,z)}{\partial t} = -\frac{1}{RT}\frac{\partial\left(u(t,z)p_i(t,z)\right)}{\partial z} - (1-\varepsilon)\rho\frac{\partial q_i(t,z)}{\partial t}; \quad i = 1,2,...n \qquad (1)$$

In the equation (1), t is the time, z is the distance along the adsorber, ρ is the framework density, ε is the bed voidage, and u is the superficial gas velocity. The molar loadings of the species i, $q_i(z,t)$ at any

position z, and time t are determined from IAST calculations. The adsorber bed is initially free of adsorbates, i.e. we have the initial condition

$$t = 0; \quad q_i(0,z) = 0$$

At time, t = 0, the inlet to the adsorber, z = 0, is subjected to a step input of the 6-component gas mixture and this step input is maintained till the end of the adsorption cycle when steady–state conditions are reached.

$$t \geq 0; \quad p_i(0,t) = p_{i0}; \quad u(0,t) = u_0$$

where u_0 is the superficial gas velocity at the inlet to the adsorber. Invoking the constraint of negligible pressure drop, the overall material balance is obtained by summing equation (1) over the six component species.

$$\frac{1}{RT} p_t \frac{\partial(u(t,z))}{\partial z} = -(1-\varepsilon)\rho \frac{\partial q_t(t,z)}{\partial t} \qquad (2)$$

Equation (2) allows the calculation of the gas velocity u along the length of the adsorber. In the breakthrough calculation the following parameter values were used: L = 0.12 m; ε = 0.75; u = 0.00225 m s^{-1} (at inlet). The framework density of **UTSA-35a** is 1046 kg m^{-3}.

Synthesis and characterization of the organic building block (H_3BTN)

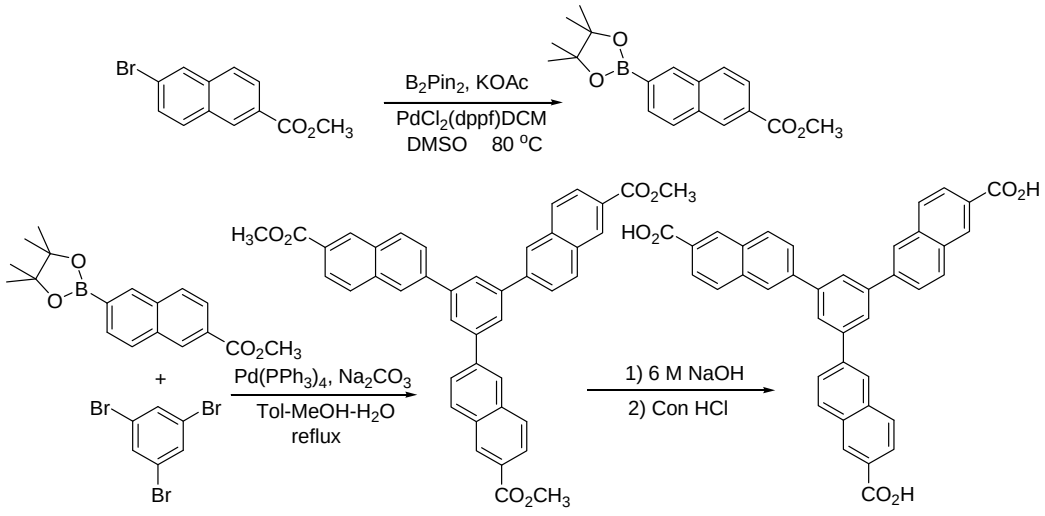

Scheme S1. Synthetic route to the organic building block H_3BTN.

Methyl 6-(pinacolboryl)-2-naphthoate: A mixture of methyl 6-bromo-2-naphthoate (15.00 g, 56.58 mmol, Alfa), B_2Pin_2 (15.80 g, 62.22 mmol, Aldrich), KOAc (16.66 g, 169.76 mmol, Aldrich) and

$PdCl_2(dppf)\cdot CH_2Cl_2$ (1.38 g, 1.69 mmol, Alfa) in dry DMSO (340 mL) was heated with stirring at 80 ^oC for 12 h under a nitrogen atmosphere. After removal of the solvents, CH_2Cl_2 (400 mL) and H_2O (200 mL) were added. The organic layer was separated and the aqueous phase was extracted with CH_2Cl_2 (100 mL × 2). The combined organic phase was washed with brine (150 mL), dried over anhydrous $MgSO_4$, filtered and concentrated to dryness. The residue was purified by silica gel column chromatography using hexane/ethyl acetate as eluent to give methyl 6-(pinacolboryl)-2-naphthoate as a pure white solid in 91% yield (16.07 g, 51.48 mmol). ^1H NMR ($CDCl_3$, 300.0 MHz) δ (ppm): 8.60 (s, 1H), 8.40 (s, 1H), 8.06 (dd, J = 8.4 Hz, 1.8 Hz, 1H), 7.91-7.94 (m, 3H), 4.00 (s, 3H), 1.42 (s, 12H); ^{13}C NMR ($CDCl_3$, 75.4 MHz) δ (ppm): 167.03, 135.72, 134.64, 133.88, 131.06, 130.69, 128.74, 128.23, 128.16, 125.07, 84.12, 52.31; selected FTIR (neat, cm^{-1}): 2976, 1709, 1598, 1485, 1437, 1379, 1338, 1287, 1268, 1230, 1177, 1129, 1095, 1080, 963, 917, 854, 842, 821, 779, 757, 703, 686, 672.

1,3,5-tri(6-methoxycarbonylnaphthalen-2-yl)benzene: To a mixture of 1,3,5-tribromobenzene (3.00 g, 9.53 mmol, Aldrich), methyl 6-(pinacolboryl)-2-naphthoate (11.90 g, 38.12 mmol), Na_2CO_3 (12.12 g, 114.35 mmol, Alfa), and $Pd(PPh_3)_4$ (1.10 g, 0.95 mmol, TCI) were added degassed toluene–methanol–water mixed solvents (200/60/60 mL). The resulting reaction mixture was stirred for 48 h under reflux under a nitrogen atmosphere. After removal of the solvents, the residue was extracted with CH_2Cl_2 (100 × 3 mL), washed with brine (80 mL), dried over anhydrous $MgSO_4$, filtrated, and concentrated in *vacuo*. The residue was purified by silica gel column chromatography using dichloromethane as eluent to give 1,3,5-tri(6-methoxycarbonylnaphthalen-2-yl)benzene as a white solid in 88% yield (5.27 g, 8.36 mmol). ^1H NMR ($CDCl_3$, 300.0 MHz) δ (ppm): 8.68 (s, 3H), 8.23 (s, 3H), 8.08-8.15 (m, 9H), 7.94-8.01 (m, 6H), 4.03 (s, 9H); ^{13}C NMR ($CDCl_3$, 75.4 MHz) δ (ppm): 166.99, 142.04, 140.37, 135.66, 131.76, 130.75, 130.03, 128.35, 127.54, 126.31, 126.09, 125.85, 125.82, 52.35; selected FTIR (neat, cm^{-1}): 2951, 1716, 1630, 1591, 1482, 1435, 1388, 1333, 1279, 1246, 1206, 1181, 1135, 1097, 1047, 993, 958, 910, 868, 804, 783, 769, 746, 700, 673.

1,3,5-tri(6-hydroxycarbonylnaphthalen-2-yl)benzene (H_3BTN): To 1,3,5-tri(6-methoxycarbonyl naphthalen-2-yl)benzene (5.00 g, 7.93 mmol) in MeOH/THF (100/50 mL) was added 6 M NaOH aqueous solution (60 mL, 360 mmol). The resulting mixture was refluxed overnight. After removal of the solvents, the residue was dissolved in water and filtered. The filtrate was neutralized with concentrated HCl (36%) in ice-water bath. The precipitation was collected by filtration, washed with water and dried in *vacuo* at 90 ^oC to give the organic building block H_3BTN as an off-white solid in

99% yield (4.61 g, 7.83 mmol). ^{1}H NMR (DMSO-d_6, 300.0 MHz) δ (ppm): 13.13 (s, 3H), 8.66 (d, J = 15.6 Hz, 6H), 8.35 (s, 3H), 8.24-8.32 (m, 6H), 8.16 (d, J = 8.7 Hz, 3H), 8.03-8.06 (m, 3H); ^{13}C NMR (DMSO-d_6, 75.4 MHz) δ (ppm): 167.21, 141.15, 139.35, 135.19, 131.47, 130.19, 129.88, 128.50, 128.10, 126.31, 125.68, 125.54; selected FTIR (neat, cm^{-1}): 1679, 1625, 1575, 1512, 1481, 1438, 1401, 1239, 1201, 1131, 957, 909, 870, 806, 770, 749, 715.

Synthesis and characterization of UTSA-35

A mixture of the organic linker H_3BTN (10 mg, 17.0 μmol) and $Cd(NO_3)_2 \cdot 4H_2O$ (20 mg, 64.8 μmol) was dissolved in DMF (1.5 mL) and heated in a disposable scintillation vial (20 mL) at 100 ^{o}C for 24 h. The block-shaped crystals were collected in 66% yield. **UTSA-35** was best formulated as $Cd_3(BTN)_2(H_2O)_3(DMF)_6$ on the basis of the single-crystal structure determination, TGA, and microanalysis. Selected FTIR (neat, cm^{-1}): 1645, 1543, 1478, 1437, 1386, 1253, 1214, 1093, 918, 874, 816, 780, 751, 704; TGA data: Calcd. weight loss for 6DMF and 3H_2O: 24.6%, Found: 24.9%; Anal. for $C_{96}H_{90}N_6O_{21}Cd_3$: C, 57.62; H, 4.53; N, 4.20, Found: C, 57.55%; H, 4.62%; N, 4.11%.

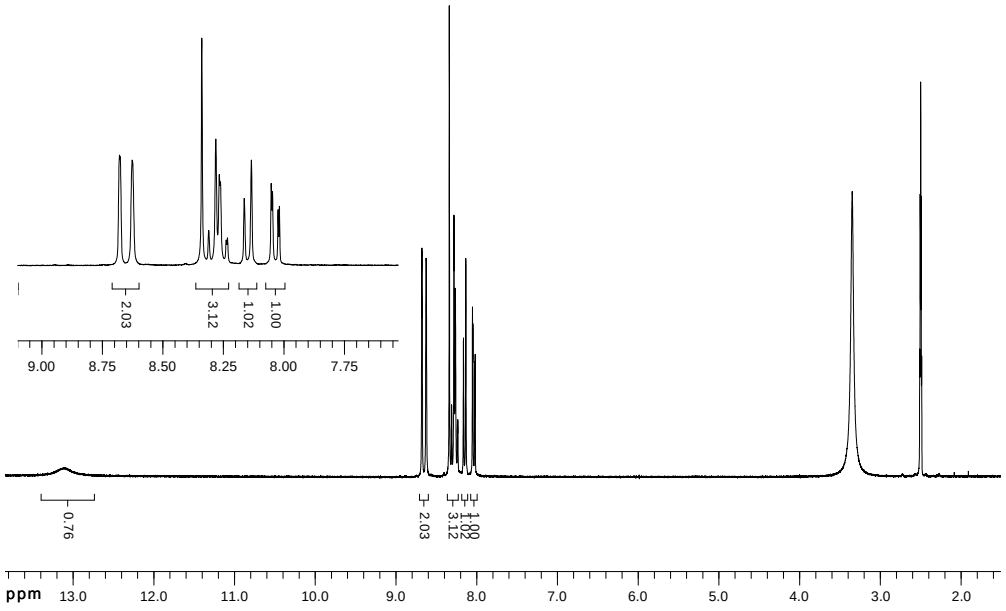

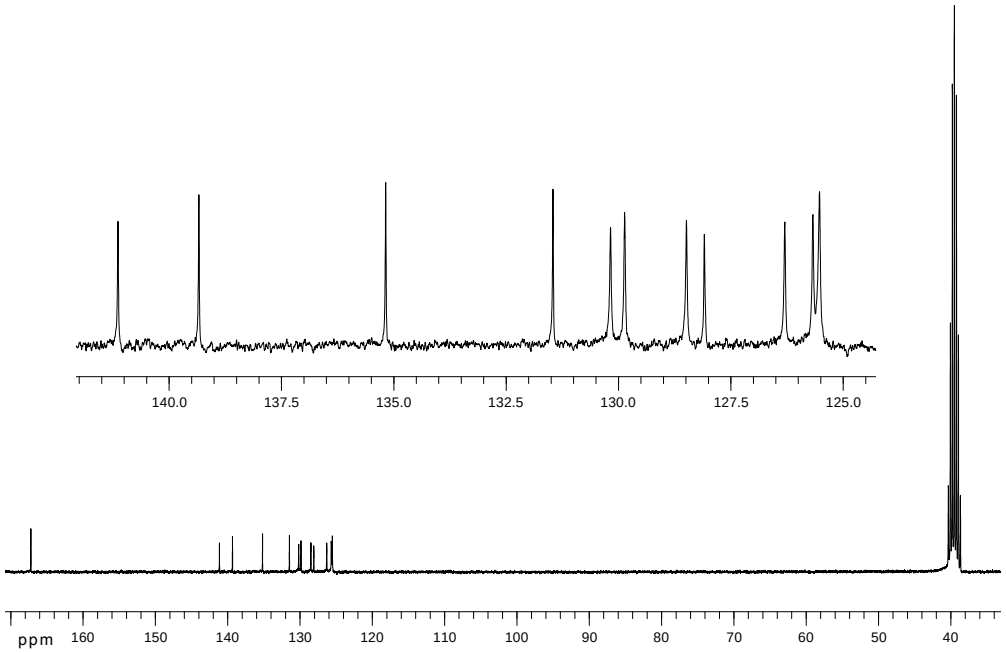

Figure S0. ^{1}H NMR (DMSO-d_6, 300.0 MHz) and ^{13}C NMR (DMSO-d_6, 75.4 MHz) spectra of the organic linker H_3BTN.

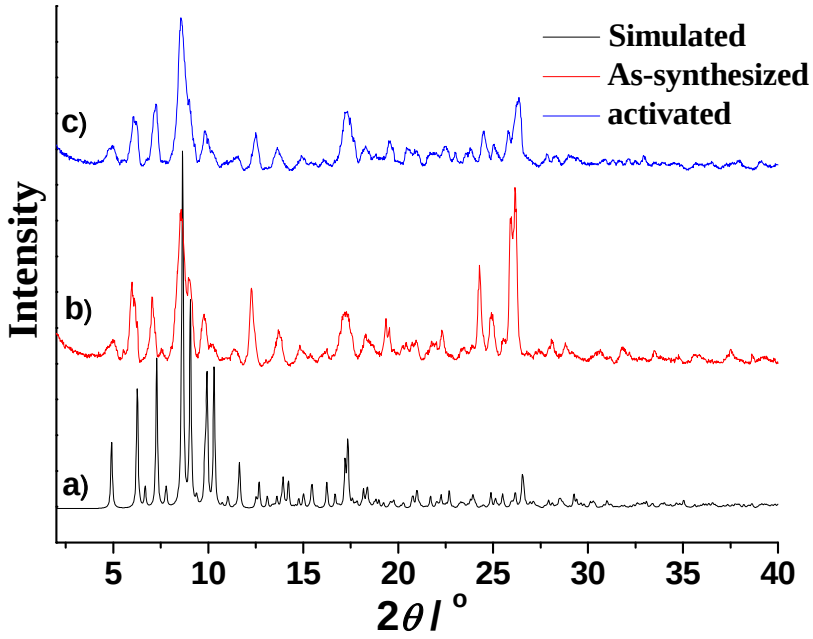

Figure S1. PXRD patterns of as-synthesized **UTSA-35** (b) and activated **UTSA-35a** (c) along with the simulated XRD pattern from its single–crystal X–ray structure (a).

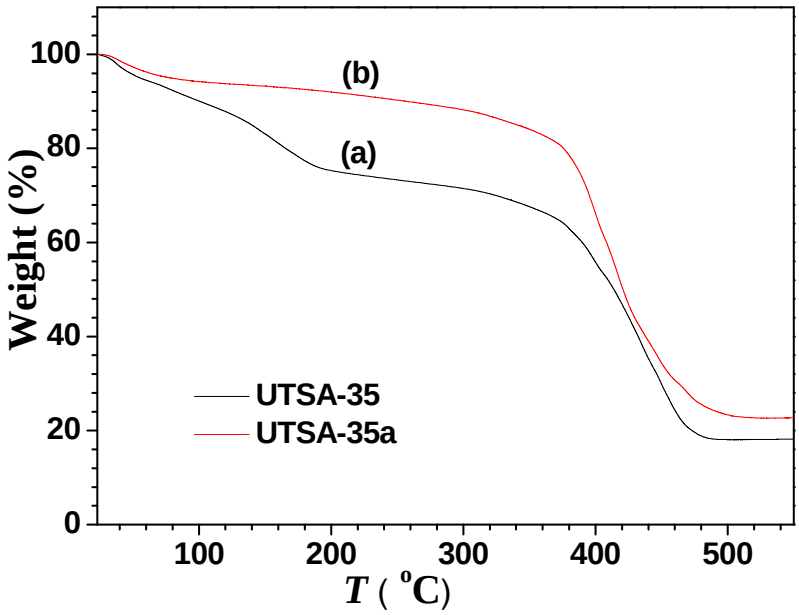

Figure S2. TGA curves of as–synthesized **UTSA-35** (a) and activated **UTSA-35a** (b).

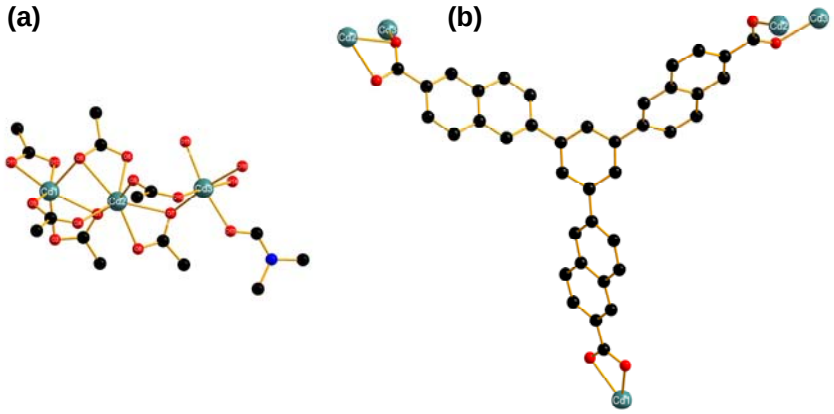

Figure S3. The tricadmium–carboxylate cluster (a) and the different coordination modes (η^2, μ_2-η^1:η^1, μ_2-η^2:η^1) of three carboxylate groups of the organic linker (b).

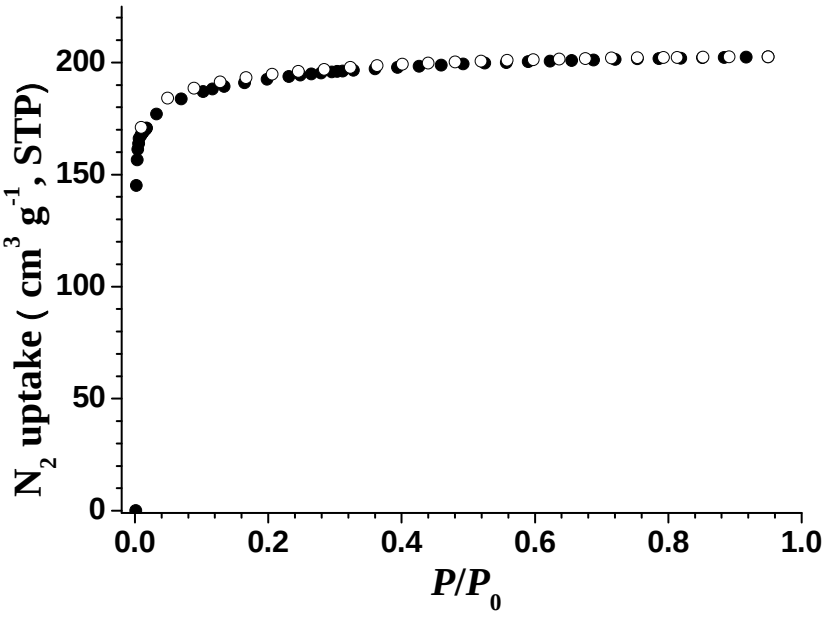

Figure S4. N_2 sorption isotherm of **UTSA-35a** at 77 K. Solid symbols: adsorption, open symbols: desorption.

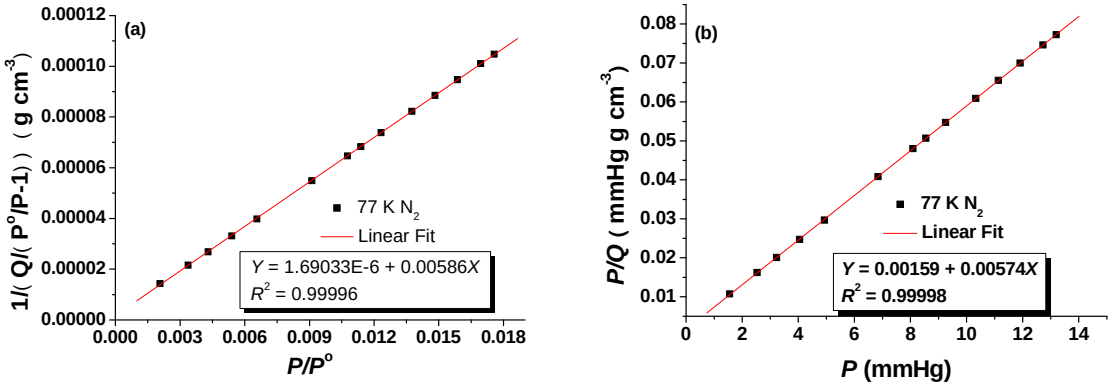

$$S_{BET} = (1/(1.69033 \times 10^{-6} + 0.00586))/22414 \times 6.023 \times 10^{23} \times 0.162 \times 10^{-18} = 742.7\ m^2\ g^{-1}$$

$$S_{Langmuir} = (1/0.00574)/22414 \times 6.023 \times 10^{23} \times 0.162 \times 10^{-18} = 758.4\ m^2\ g^{-1}$$

$$\text{BET constant} = 1 + 0.00586/(1.69033 \times 10^{-6}) = 3467.8$$

$$\text{Langmuir constant} = 0.00574/0.00159 = 3.6\ mmHg^{-1} = 2.7 \times 10^{-2}\ Pa^{-1}$$

Figure S5. The BET (a) and Langmuir (b) surface areas of **UTSA-35a** obtained from N_2 adsorption isotherm at 77 K.

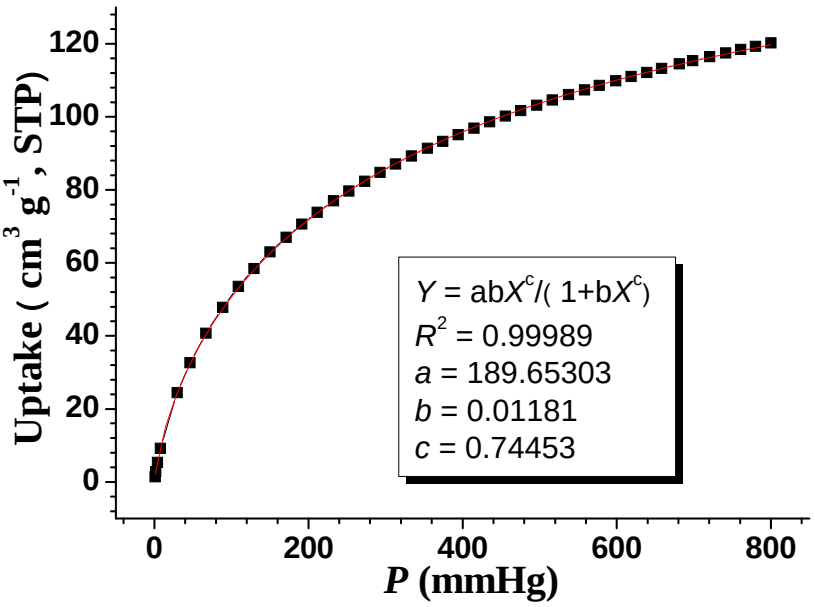

Figure S6. Fitting the hydrogen isotherm data with Langmuir–Freudlium equation, from which the maximum H_2 adsorption amount of 189.7 $cm^3 g^{-1}$ (STP) (1.7 wt%) at 77 K can be predicted.

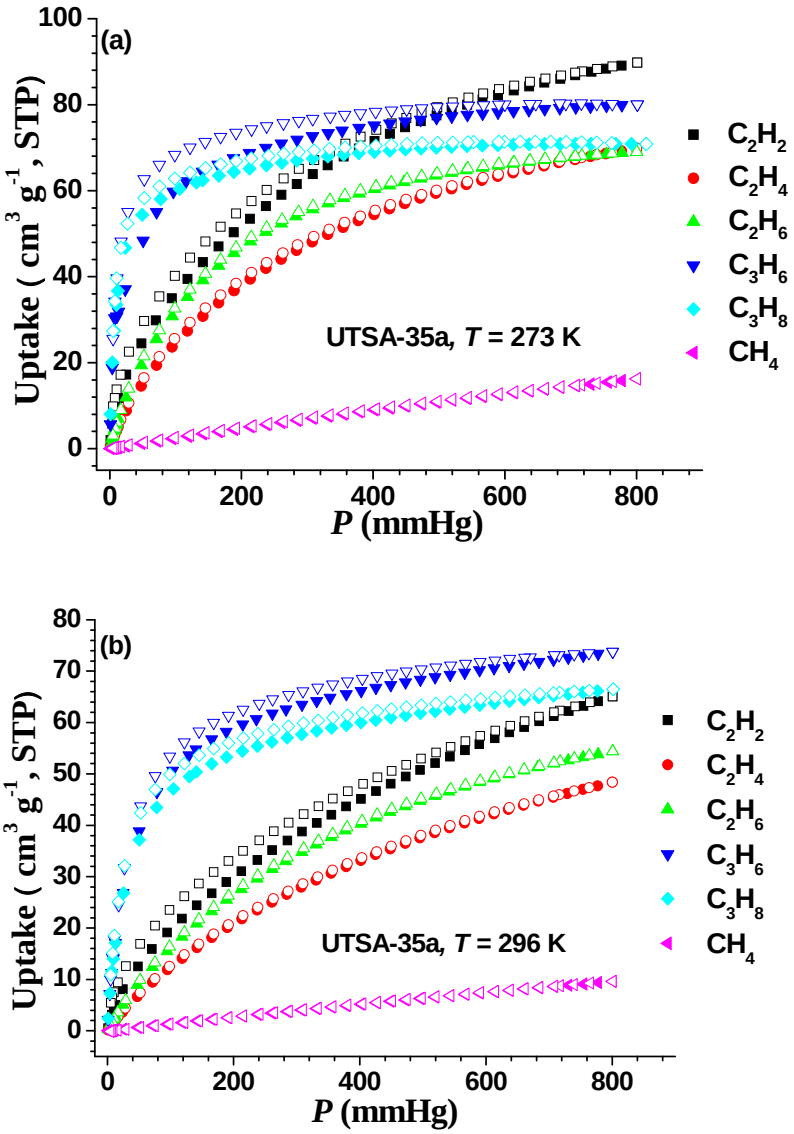

Figure S7. Single–component sorption isotherms of various hydrocarbons in **UTSA-35a** at 273 K (a), and 296 K (b). Solid symbols: adsorption, open symbols: desorption.

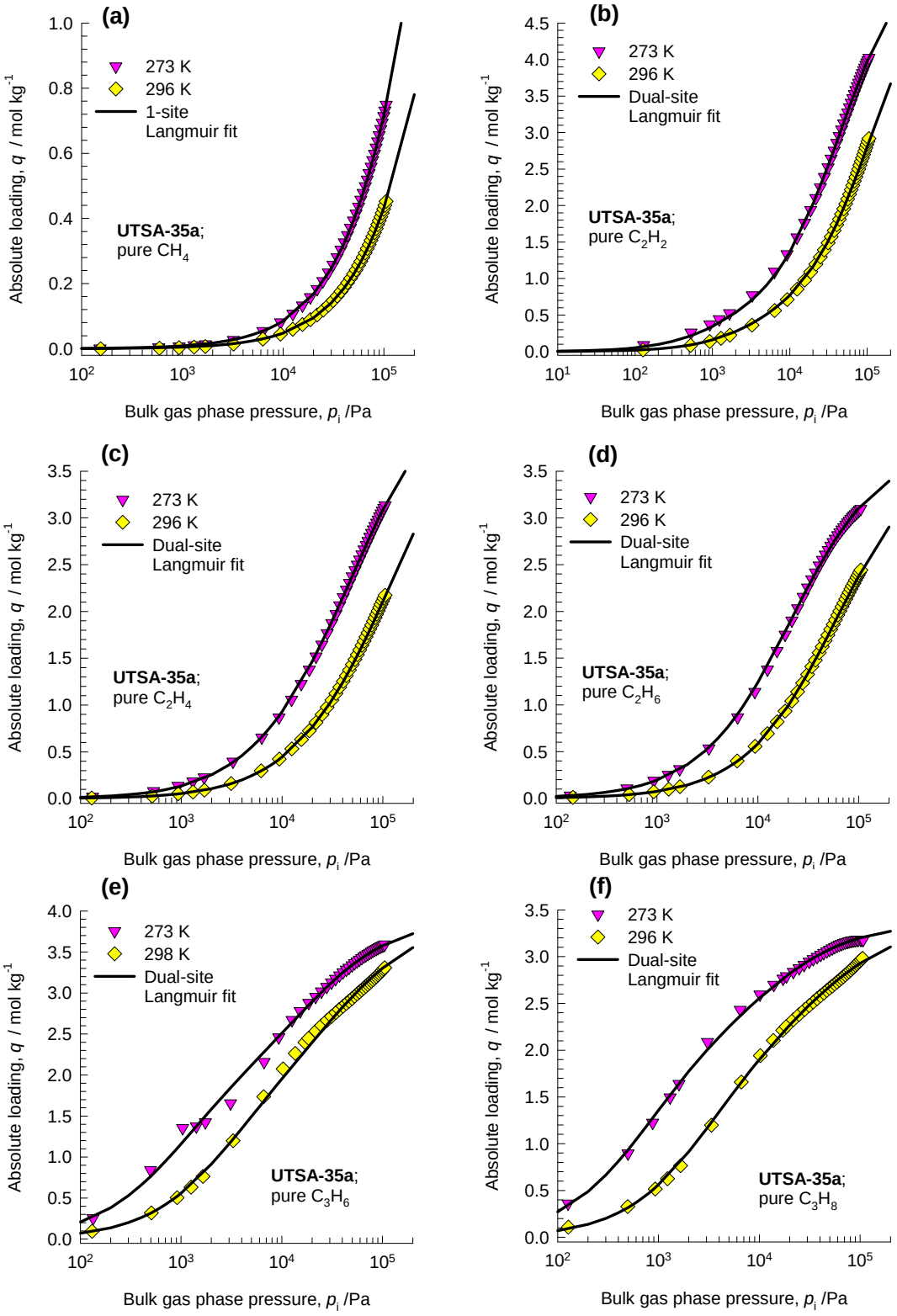

Figure S8. Comparison of the experimentally determined absolute loadings with the Langmuir isotherm fits. The continuous solid lines are the Langmuir fits using the parameters in *Table S2*.

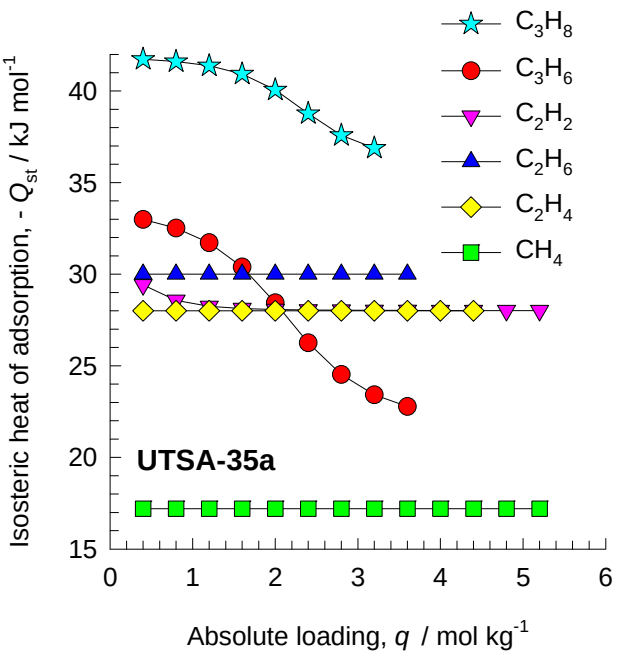

Figure S9. Comparison of the loading dependences of the isosteric heats of adsorption of different hydrocarbons in **UTSA-35a**.

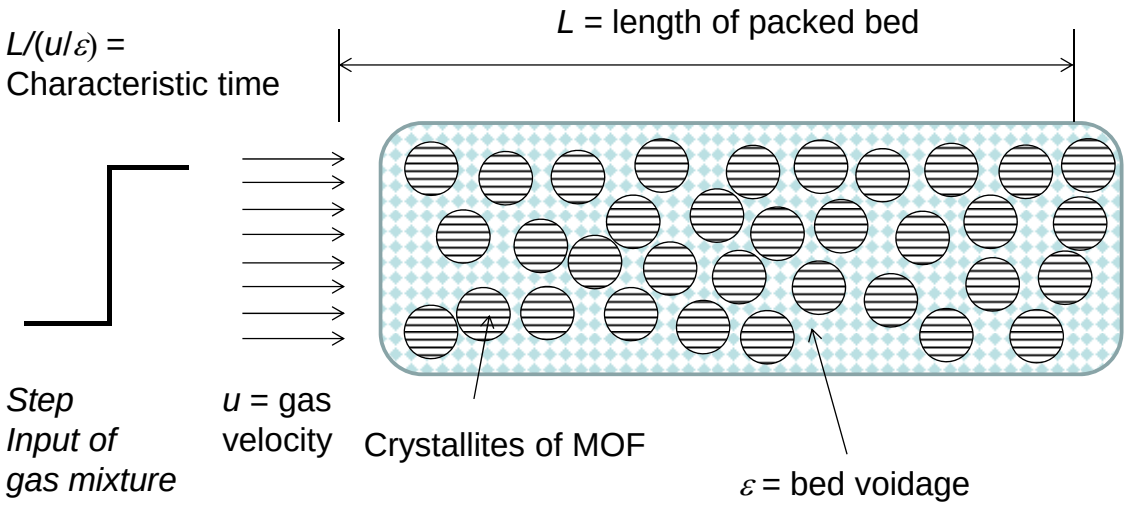

Figure S10. Schematic of a packed bed adsorber.

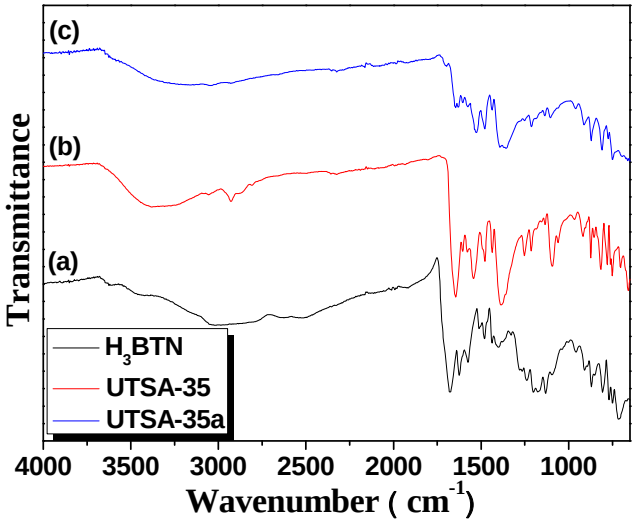

Figure S11. FTIR spectra of the organic building block H_3BTN (a), as–synthesized **UTSA-35** (b) and activated **UTSA-35a** (c).

Table S1. Crystal data and structure refinement for **UTSA-35**

Empirical formula	$C_{84}H_{62}Cd_3N_2O_{17}$
Formula weight	2001.00
Temperature (K)	100(2)
Wavelength (Å)	0.71073
Crystal system, space group	Monoclinic, $P2_1/c$
Unit cell dimensions	a = 14.306(2) Å α = 90° b = 19.509(3) Å β = 99.6290(9)° c = 36.482(5) Å γ = 90°
Volume (Å^3)	10039(2)
Z, Calculated density (Mg m^{-3})	4, 1.324
Absorption coefficient (mm^{-1})	0.683
F(000)	3440
Crystal size (mm)	0.37 × 0.20 × 0.17
θ range for data collection	2.55 to 25.66°
Limiting indices	$-17 \le h \le 17$, $-23 \le k \le 23$, $-44 \le l \le 44$
Reflections collected / unique	32711 / 18251 (R_{int} = 0.0513)
Completeness to θ = 25.66°	95.8 %
Max. and min. transmission	0.8928 and 0.7862
Refinement method	Full–matrix least–squares on F^2
Data / restraints / parameters	18251 / 0 / 907
Goodness-of-fit on F^2	1.022
Final R indices [$I > 2\sigma(I)$]	R_1 = 0.0594, wR_2 = 0.1586
R indices (all data)	R_1 = 0.1090, wR_2 = 0.1744
Largest diff. peak and hole (e.Å^{-3})	1.979 and -0.901
CCDC No.	868753

Table S2. Isotherm fit parameters for **UTSA-35a**.

Adsorbate	Site A			Site B		
	$q_{sat,A}$ mol kg^{-1}	b_{A0} Pa^{-1}	E_A kJ mol^{-1}	$q_{sat,B}$ mol kg^{-1}	b_{B0} Pa^{-1}	E_B kJ mol^{-1}
CH_4	4	1.12×10^{-9}	17.2			
C_2H_2	5.05	9.7×10^{-11}	28	0.5	1.04×10^{-9}	31
C_2H_4	4	8.33×10^{-11}	28	0.5	6.08×10^{-10}	28
C_2H_6	3.65	8.45×10^{-11}	30	0.1	9.02×10^{-10}	30
C_3H_6	1.8	3.78×10^{-9}	21.5	2.1	3.28×10^{-10}	34
C_3H_8	1.11	9.37×10^{-12}	36	2.25	1.22×10^{-11}	42

Notation

b_i	dual-site Langmuir constant for species i, Pa^{-1}
L	length of packed bed adsorber, m
n	number of components in mixture, dimensionless
p_i	bulk gas pressure of species i, Pa
q_i	component molar loading of species i, mol kg^{-1}
q_t	total mixture loading, mol kg^{-1}
$q_{i,sat}$	saturation loading of species i, mol kg^{-1}
t	time, s
T	temperature, K
u	superficial gas velocity, m s^{-1}

Greek letters

ε	voidage of packed bed, dimensionless
τ	dimensionless time
τ_{break}	breakthrough time, dimensionless

Subscripts

i	referring to component i
A	referring to site A
B	referring to site B

Reference

[1] Mason, J. A., Sumida, K., Herm, Z. R., Krishna, R. & Long, J. R. Evaluating Metal–Organic Frameworks for Post-Combustion Carbon Dioxide Capture *via* Temperature Swing Adsorption. *Energy Environ. Sci.* **3**, 3030–3040 (2011).

[2] Myers, A. L. & Prausnitz, J. M. Thermodynamics of mixed gas adsorption. *A.I.Ch.E.J.* **11**, 121–130 (1965).

[3] Krishna, R. & van Baten, J. M. Using molecular simulations for screening of zeolites for separation of CO_2/CH_4 mixtures. *Chem. Eng. J.* **133**, 121–131 (2007).

[4] Krishna, R. & van Baten, J. M. In Silico Screening of Zeolite Membranes for CO_2 Capture. *J. Membr. Sci.* **360**, 323–333 (2010).

[5] Krishna, R. & van Baten, J. M. In silico screening of metal–organic frameworks in separation applications. *Phys. Chem. Chem. Phys.* **13**, 10593–10616 (2011).

[6] Krishna, R. & Long, J. R. Screening metal–organic frameworks by analysis of transient breakthrough of gas mixtures in a fixed bed adsorber. *J. Phys. Chem. C* **115**, 12941–12950 (2011).

[7] Krishna, R. & van Baten, J. M. A comparison of the CO_2 capture characteristics of zeolites and metal–organic frameworks. *Sep. Purif. Technol.* **87**, 120–126 (2012).

[8] Krishna, R. & Baur, R. Modelling issues in zeolite based separation processes. *Sep. Purif. Technol.* **33**, 213–254 (2003).